Journal of
Polymer Materials

Tech Science Press

Doi:10.32604/jpm.2025.065320

ARTICLE

Synergistic Effect of Silicone Macromolecular Charring Agent and Ammonium Polyphosphate on Improving Flame Retardancy and Mechanical Properties of Ethylene-Butyl Acrylate Copolymer Composites

Xuan Huo[1], Bingchen Wu[1], Yuanmeng Lou[1], Junlin Zhu[1], Cui Li[1], Lili Ma[1], Ye-Tang Pan[2], Chuncheng Hao[1,*] and Xin Wen[1,*]

[1]College of Materials Science and Engineering, Qingdao University of Science and Technology, Qingdao, 266042, China
[2]National Engineering Research Center of Flame Retardant Materials, School of Materials Science & Engineering, Beijing Institute of Technology, Beijing, 100081, China

*Corresponding Authors: Chuncheng Hao. Email: hao@qust.edu.cn; Xin Wen. Email: hgwenxin@qust.edu.cn

Received: 10 March 2025; Accepted: 27 May 2025; Published: 11 July 2025

ABSTRACT: Power cables are important pieces of equipment for energy transmission, but achieving a good balance between flame retardancy and mechanical properties of cable sheaths remains a challenge. In this work, a novel intumescent flame retardant (IFR) system containing silicone-containing macromolecular charring agent (Si-MCA) and ammonium polyphosphate (APP) was designed to synergistically improve the flame retardancy and mechanical properties of ethylene-butyl acrylate copolymer (EBA) composites. The optimal mass ratio of APP/Si-MCA was 3/1 in EBA composites (EBA/APP-Si-31), corresponding to the best flame retardancy with 31.2% of limited oxygen index (LOI), V-0 rating in UL-94 vertical burning test, and 76.4% reduction on the peak of heat release rate (PHRR) in cone calorimeter test. The enhancement mechanism was attributed to the synergistic effect of APP/Si-MCA during combustion, including the radical-trapping effect, the dilution effect of non-flammable gases, and the barrier effect of the intumescent char layer. Meanwhile, the tensile results indicated that EBA/APP-Si-31 also exhibited good mechanical properties with the addition of maleic anhydride-grafted polyethylene (PE-*g*-MA) as the compatibilizer. Thus, the APP/Si-MCA combination is an effective IFRs system for preparing high-performance EBA composites, and it will promote their applications as cable sheath materials.

KEYWORDS: Ethylene-butyl acrylate copolymer; intumescent flame retardants; polymer composites; synergistic effect; cable sheath

1 Introduction

Power cables play a vital role in energy transmission, and they are closely linked to system security [1–4]. In the structure of cables, the sheaths are composed of organic polymers [5–7], which generally include polyvinyl chloride (PVC), polyethylene (PE), polypropylene (PP), ethylene vinyl acetate (EVA), ethylene-butyl acrylate copolymer (EBA), or various polymer blends. Due to the innate flammability of polymer materials, the cable sheaths are significantly responsible for fire accidents of power cables [8–11]. In the event of a fire, it will not only lead to the interruption of power transmission and cause substantial economic losses, but also affect the health and safety of individuals [12–14]. Consequently, it is essential to improve the flame retardancy of cable sheath materials to prevent fire accidents.

Copyright © 2025 The Authors. Published by Tech Science Press.
This work is licensed under a Creative Commons Attribution 4.0 International License, which permits unrestricted use, distribution, and reproduction in any medium, provided the original work is properly cited.

To achieve the satisfactory flame retardancy of cable sheaths, halogen-free flame retardants are preferred due to their environmental friendliness. Up to now, a great deal of excellent research has been done via the incorporation of inorganic compounds [15–17], organic additives [18,19], or their combinations [20,21]. For instance, $Mg(OH)_2$ is a typical flame retardant with the advantages of abundant resources from natural minerals, low cost and eco-friendliness [22]. Under high-temperature conditions, $Mg(OH)_2$ can generate water to absorb heat through vaporization to cool the material. Wang et al. [23] reported that when 60 wt% $Mg(OH)_2$ was added to low-density polyethylene (LDPE), the limiting oxygen index (LOI) increased from 17.5% to 25.5%. Ye et al. [24] also incorporated 60 wt% $Mg(OH)_2$ into EVA to achieve the UL-94 V0 rating in EVA composites. These results indicated the low flame retardant efficiency of $Mg(OH)_2$, which easily leads to the sacrifice of the mechanical properties of polymer composites.

Phosphorus-based flame retardants or their combinations are also widely applied for cable sheath materials. Tian et al. [25] investigated the effect of aluminum hypophosphite (AHP) on the flame retardance of LDPE. The results indicated that the incorporation of 50 phr AHP could increase the LOI to 27.5% and pass the V0 rating in the UL-94 test. Liang et al. [26] added microencapsulated red phosphorus (MRP) into the PP matrix and found that the MRP content had a significant effect on the mechanical properties of the resultant polymer composites. Wang et al. [27] prepared LDPE/10 wt% MRP/30 wt% AHP composites, which could achieve the V0 rating and formed a denser carbon layer after combustion. Meanwhile, the composites maintained a high tensile strength of over 10 MPa. In our previous work [28], the synergistic effect of nanoscale carbon black (CB) and ammonium polyphosphate (APP) on the flame retardancy of PP composites was investigated. The optimal sample designated as 7CB18APP (PP composites containing 7 wt% CB and 18 wt% APP), presented the LOI value of 29.8% and the UL-94 V0 rating.

Furthermore, intumescent flame retardants (IFRs) are important additives in the preparation of cable sheath materials. During combustion, IFRs can decompose to form an intumescent carbon layer wrapping around the surface, playing critical roles in isolating heat, combustible volatile gases, and oxygen, thus blocking the combustion process. Khanal et al. [29] reported an IFR system consisting of APP and tris (2-hydroxyethyl) isocyanurate (THEIC) to prepare high-density polyethylene (HDPE) composites. As the content of IFR increased, the LOI value gradually increased, but the elongation at break and tensile strength showed a marked downward trend. Zhang et al. [30] synthesized microencapsulated APP via a hyperbranched polyester (K-HBPE@APP) and investigated the flame-retardant effect in the PP system. Compared with adding equal amounts of K-HBPE/APP blends, the K-HBPE@APP increased not only the LOI value and UL-94 rating, but also tensile strength and the elongation at break. Ren et al. [31] synthesized M-UF (KH-550 modified urea-formaldehyde resin) and investigated the carbon-formation effect of M-UF/APP in the PP matrix. Compared with PP/30 wt% APP, PP/20 wt% APP/10 wt% M-UF had more intumescent carbon layer, resulting in better flame-retardant performances as demonstrated by both UL-94 and LOI tests.

In comparison with other cable sheaths, EBA offers several advantages in terms of flexibility, low-temperature performance, and processability. These superiorities render EBA suitable for serving as the new generation of cable sheath materials. In this study, to enhance the flame retardancy of EBA cable sheath, a novel silicone-containing macromolecular charring agent (Si-MCA) was synthesized [32], and it was combined with APP as IFRs to prepare EBA/APP/Si-MCA composites. The effect of APP/Si-MCA ratios on the flame retardancy of EBA/IFR composites was investigated by LOI, UL-94, and cone calorimeter tests. Further, the gas products and char structure were analyzed to discuss the flame retardant mechanism of APP/Si-MCA. Meanwhile, the mechanical properties of EBA/APP/Si-MCA systems were evaluated by tensile test to study the compatibilizing effect of maleic anhydride-grafted polyethylene (PE-*g*-MA).

2 Materials and Methods

2.1 Materials

Ethylene-butyl acrylate copolymer (EBA, 3427AC) powder was supplied by Dupont Co., Ltd. (America). Ammonium polyphosphate (APP) was purchased from Zhenjiang Xingxing Flame-retardant Co., Ltd. (Zhenjiang, China). Silicone-containing macromolecular charring agent (Si-MCA) was synthesized in our laboratory according to our previous literature [32]. The chemical structures of EBA and Si-MCA are shown in Fig. 1. Maleic anhydride-grafted polyethylene (PE-*g*-MA) was obtained from Zhongjie Chemical Co., Ltd. (Guangzhou, China), and the grafting degree of MA was about 0.9 wt%.

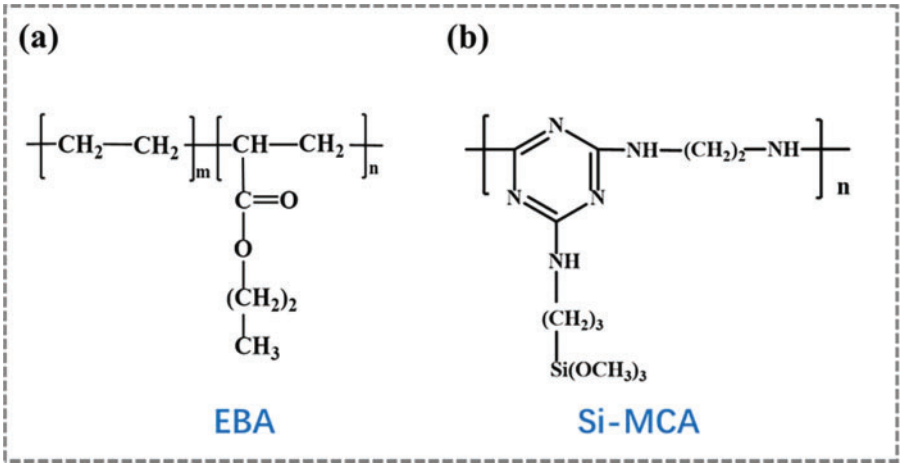

Figure 1: The chemical structures of (a) EBA, (b) Si-MCA

2.2 Preparation of EBA Composites

EBA composites were prepared via melt compounding in a Haake batch intensive mixer (Rheomix 600, Karlsruhe, Germany) at 160°C with the rotor speed of 80 rpm for 8 min. PE-*g*-MA was used as a compatibilizer at a fixed content of 10 wt%, while the IFRs content was fixed at 25 wt% in all EBA composites. For convenience, the samples were designated as EBA/APP (with only 25 wt% APP) and EBA/APP-Si-xy, where xy represents the mass ratio of APP/Si-MCA. For example, EBA/APP-Si-31 indicates APP/Si-MCA = 3/1 in EBA composites. Notably, EBA/APP-Si-31-0 was also prepared under the same conditions; it contained APP/Si-MCA = 3/1 but without PE-*g*-MA.

2.3 Characterization

The limited oxygen index (LOI) was measured on a JF-3 oxygen index meter (Jiangning, China) with sheet dimensions of 130 × 6.5 × 3.2 mm^3, in accordance with ISO4589-1984. The vertical burning test was carried out according to the UL-94 (ANSI/ASTMD635-77) with sheet dimensions of 125 × 12.7 × 3.2 mm^3. Thermogravimetric analysis (TGA) was conducted by a Q600 thermal analyzer (TA Co., New Castle, DE, USA) at a heating rate of 10°C min^{-1} in air from 25°C to 650°C. Cone calorimeter testing (iCone, FTT, West Sussex, UK) was conducted according to ISO 5660-1. The sample dimension was 100 × 100 × 6 mm^3; it was backed by aluminum foil and irradiated at a heat flux of 50 kW m^{-2}. The photographs of residual chars after cone calorimeter testing were taken by a digital camera. And the surface morphology was further observed by scanning electron microscopy (SEM, JSM-6700F, JEOL, Tokyo, Japan). The surface element analysis was

characterized by X-ray photoelectron spectroscopy (XPS, K-Alpha, Thermo Fisher, Waltham, MA, USA) and Fourier Transform Infrared spectra (FTIR 460 PLUS spectrometer, Tokyo, Japan). The TGA-FTIR instrument consists of a thermogravimeter (TG209, Netzsch Instruments Co., Selb, Germany), a Fourier transform infrared spectrometer (Tensor 27, Bruker Optics Inc., Ettlingen, Germany), and a transfer tube with an inner diameter of 1 mm connecting the TGA and the infrared cell. The investigation was carried out from 30°C to 750°C at a heating rate of 20°C/min under a nitrogen flow of 100 mL/min. Uniaxial tensile tests were performed at room temperature with an Instron 1121 testing machine (Canton, MA, USA). Specimens were compression molded into sheets with 1 mm thickness, then cut into a dumbbell shape with gauge dimensions of 20 mm × 4 mm × 1 mm. The measurements were conducted at a crosshead speed of 50 mm/min. At least five runs for each sample were measured, and the averaged data were recorded as results.

3 Results and Discussion

3.1 Flame Retardancy of EBA/IFR Composites

Firstly, the flame retardancy of neat EBA and EBA/IFR composites was studied by LOI and UL-94 tests. These two methods are the most commonly employed techniques for examining the combustion behavior and fire-resistance capabilities [33–36]. As listed in Table 1, the LOI value of neat EBA was only 17.5%, while that of EBA/APP could reach 21.4%. Meanwhile, it was apparent that the combinations of APP/Si-MCA exhibited higher LOI values. With the decreasing mass ratios of APP/Si-MCA from 5/1 to 3/1, the LOI gradually increased from 24.5% to 31.2%. However, when the APP/Si-MCA ratio further decreased to 2/1, the LOI decreased to 30.6%. Moreover, although both APP and APP/Si-MCA had a positive effect on inhibiting the melt dripping of EBA, only EBA/APP-Si-31 and EBA/APP-Si-21could reach the UL-94 V0 rating. Notably, the extinction time ($t_1 + t_2$) of EBA/APP-Si-31 was shorter than that of EBA/APP-Si-21, indicating better flame retardancy. Thus, the optimal sample was EBA/APP-Si-31, which displayed the highest LOI value and the UL-94 V0 rating with the shortest extinction time among EBA samples.

Table 1: Combustion parameters of EBA samples from LOI, UL-94, and cone calorimeter tests

Samples	IFRs (25 wt%)	LOI (%)	UL-94 (3.2 mm)		
	APP/Si-MCA		$t_1 + t_2$ (s)	Dripping	Rating
EBA	–	17.5 ± 0.2	>30	Yes	NR
EBA/APP	–	21.4 ± 0.3	>30	No	NR
EBA/APP-Si-51	5/1	24.5 ± 0.2	3 + 45	No	NR
EBA/APP-Si-41	4/1	27.8 ± 0.2	3 + 23	No	V1
EBA/APP-Si-31	3/1	31.2 ± 0.3	2 + 4	No	V0
EBA/APP-Si-21	2/1	30.6 ± 0.3	2 + 7	No	V0

Subsequently, thermogravimetric analysis (TGA) was used to investigate the thermal stability of EBA samples, which is able to indirectly evaluate the flame retardancy of polymer materials. As shown in Fig. 2a, the thermal decomposition temperature of EBA/APP shifted to a lower temperature range, which can be attributed to the low-temperature thermal decomposition characteristics of APP. In contrast, EBA/APP-Si-31 shifted to a higher temperature compared with EBA/APP, suggesting the combination of APP/Si-MCA enhanced the thermal stability of EBA. Meanwhile, Table 2 exhibits similar trends for $T_{5wt\%}$ and $T_{10wt\%}$, which are the characteristic temperatures corresponding to 5 and 10 wt% mass loss, respectively. Furthermore, derivative thermogravimetry (DTG) curves in Fig. 2b also confirmed the trend of a decrease

followed by an increase for T_{max} (corresponding to the maximum mass loss rate). Notably, the degradation rate at T_{max} was different. EBA/APP-Si-31 displayed the lowest degradation rate, thereby indicating the best thermal stability. Additionally, the higher amount of char residue from EBA/APP-Si-31 implied excellent carbonization ability of APP/Si-MCA, which is conducive to the formation of a high-quality char layer with better flame retardancy [28].

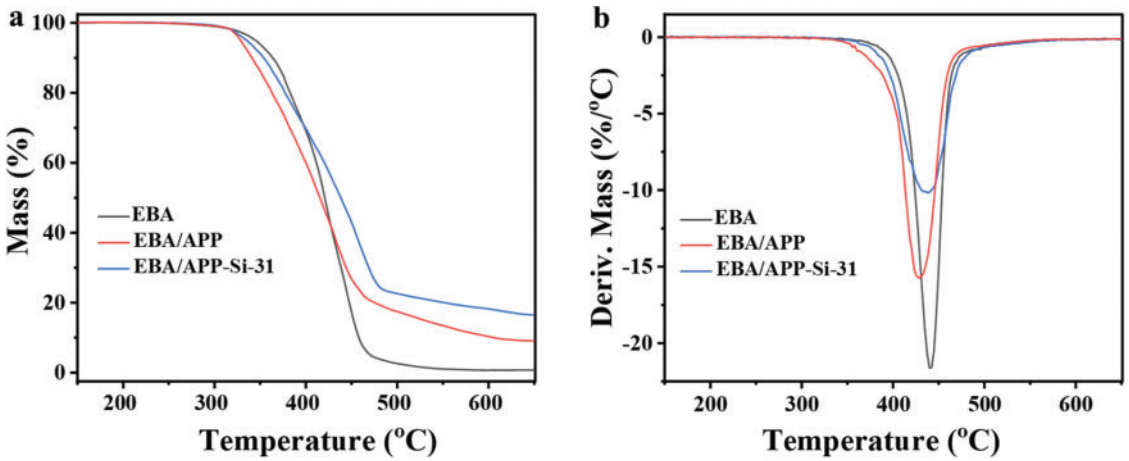

Figure 2: TGA (a) and DTG (b) curves of neat EBA and its composites in air

Table 2: Thermal decomposition properties of neat EBA and its composites in air

Samples	$T_{5wt\%}$ (°C)	$T_{10wt\%}$ (°C)	T_{max} (°C)	Residue at 650°C
EBA	345.9	363.7	441.2	0
EBA/APP	328.2	341.5	428.8	9.2%
EBA/APP-Si-31	335.6	354.9	437.6	16.4%

The flame retardancy of EBA samples was further investigated by cone calorimeter testing (CCT), which is helpful for providing important combustion parameters related to fire risk [37–39], such as time to ignition (TTI), heat and smoke release, CO production, mass loss, etc. Fig. 3a shows heat release rate (HRR)—combustion time curves for neat EBA, EBA/APP, and EBA/APP-Si-31, while their detailed fire parameters are summarized in Table 3. It was found that the TTI values of EBA/APP and EBA/APP-Si-31 became shorter, implying that they were easier to ignite than neat EBA. However, a significant decrease in the peaks of HRR (PHRRs) was observed. The PHRR values from EBA/APP and EBA/APP-Si-31 were 604 and 305 kW/m^2, respectively, which were reduced by 53.3% and 76.4% in comparison with neat EBA (1293 kW/m^2). Furthermore, Fig. 3b illustrates their curves of total heat release (THR). Significantly, the slope of the THR curve became flatter, and the final THR value became smaller. Especially, the THR of EBA/APP-Si-31 decreased by 40.2% compared to neat EBA. These results suggested that APP-Si-31 was effective in reducing heat release and suppressing the fire spread in EBA composites.

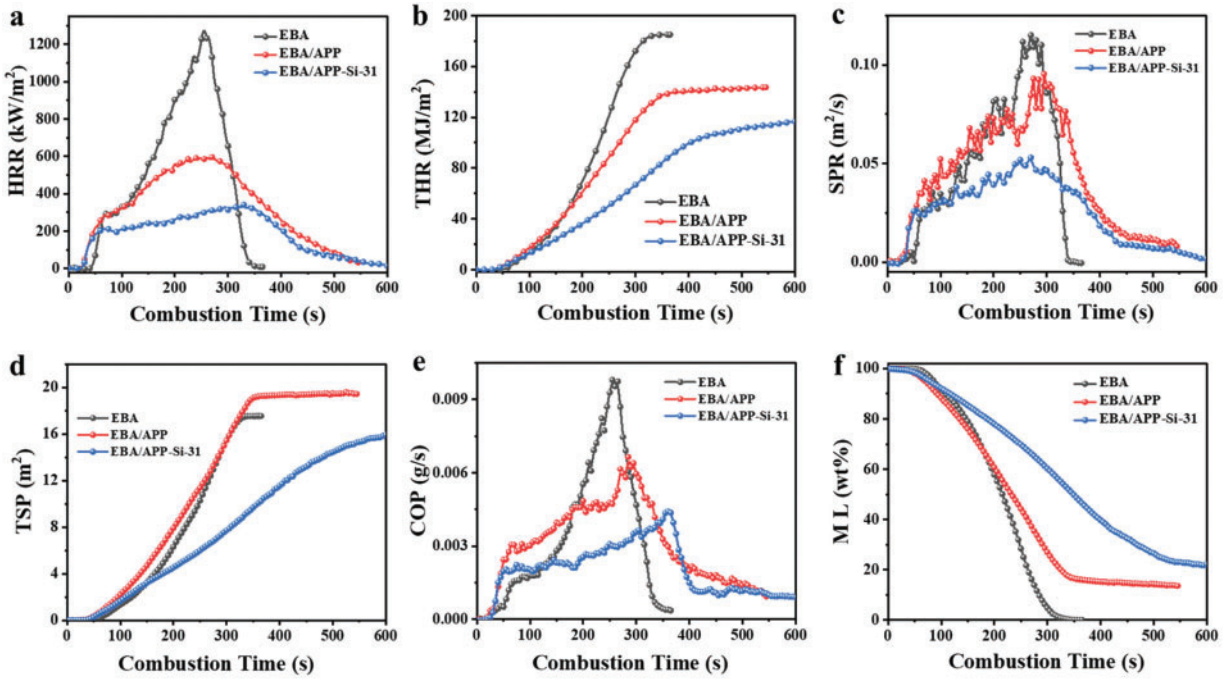

Figure 3: (a) HRR, (b) THR, (c) SPR, (d) TSP, (e) COP, and (f) normalized ML curves of EBA samples

Table 3: Cone calorimetry testing data for EBA samples at 50 kW/m^2

Samples	TTI[a] (s)	PHRR[b] (kW/m^2)	THR[c] (MJ/m^2)	TSP[d] (m^2/m^2)	PCOP[e] (g/s)	Char (wt%)
EBA	49	1293	184.9	17.5	0.0098	0
EBA/APP	30	604	176.2	19.4	0.0064	13.6
EBA/APP-Si-31	31	335	110.6	15.8	0.0044	22.1

Note: [a]TTI: time to ignition; [b]PHRR: peak of heat release rate; [c]THR: total heat release; [d]TSP: total smoke production; [e]PCOP: peak of CO production.

Besides heat release, the smoke and CO releases are also important to evaluate fire hazard. It is reported that the acute toxicity of fire gases is mainly responsible for over 70% of people killed by fires [40–42]. As shown in Fig. 3c, the peak of the smoke production rate (PSPR) of EBA/APP-Si-31 was lower than that of neat EBA and EBA/APP. Meanwhile, the total smoke production (TSP) of EBA/APP-Si-31 was also lower than that of the others (Fig. 3d). Moreover, according to CO production curves in Fig. 3e, EBA/APP-Si-31 exhibited a dramatic reduction in the peak of CO production (PCOP). Correspondingly, here the less smoke and CO releases were favorable for decreasing the toxicity of fire gases and providing more escaping time.

Finally, Fig. 3f shows normalized mass loss curves of EBA samples with combustion time. Compared to neat EBA, EBA/APP and EBA/APP-Si-31 displayed relatively flatter curves with smaller slopes, implying their weaker fire intensity. Meanwhile, the percentage values of residual char were different (Table 3). As a non-charring polymer, the residual char of neat EBA was nearly zero. The char residue of EBA/APP was 13.6 wt% due to the solid product derived from APP. Interestingly, the residual char of EBA/APP-Si-31 was as high as 22.1 wt%, which was ascribed to the crosslinked carbonization of APP and Si-MCA to form an IFR char layer. As is known, once more char is formed in the condensed-phase region, the amount of flammable

fuels entering the gas-phase region will be greatly reduced, resulting in decreased thermal and smoke releases during combustion.

3.2 Flame Retardant Mechanism Analysis for EBA/IFR Composites

To investigate the flame-retardant mechanism, TGA-FTIR was employed to analyze the gas-phase products of neat EBA and EBA/APP-Si-31. As shown in Fig. 4a,b, it was found that most gas products were similar, but EBA/APP-Si-31 had weaker absorption intensities. Meanwhile, the FTIR spectra of their gaseous products at different temperatures were comparatively studied. When the temperature exceeded 400°C, the characteristic absorption peaks of H_2O (3810–3640 cm^{-1}), C-H (2970–2940 cm^{-1}), CO_2 (2370–2340 cm^{-1}), C=O (1749 cm^{-1}) and C-H (1510 cm^{-1}) were detected (Fig. 4c). These peaks should be assigned to the thermal decomposition products of EBA. In the case of EBA/APP-Si-31, these characteristic absorption peaks of EBA appeared with weaker intensities, and a new peak for P-O at 958 cm^{-1} was observed (Fig. 4d). The peak intensities for hydrocarbons, carbonyl compounds and C-H were greatly decreased, indicating most carbon elements were fixed in solid chars. Specifically, the almost disappeared peak for CO and the newly appeared P=O peak confirmed the reduced toxicity and the flame retardant effect from the P element. In addition, the FTIR spectra of gaseous products at the maximum degradation stage were analyzed. As shown in Fig. 4e, weaker peaks for these molecular fuels and the characteristic peaks for P=O (1239 cm^{-1}), P-C (1057 cm^{-1}), and P-O-C (925 cm^{-1}) were visible [43,44]. Here, the presence of P-containing groups was attributed to PO•/HPO• radicals released from APP during combustion, which could effectively quench reactive H• and HO• radicals, thereby inhibiting combustion reactions.

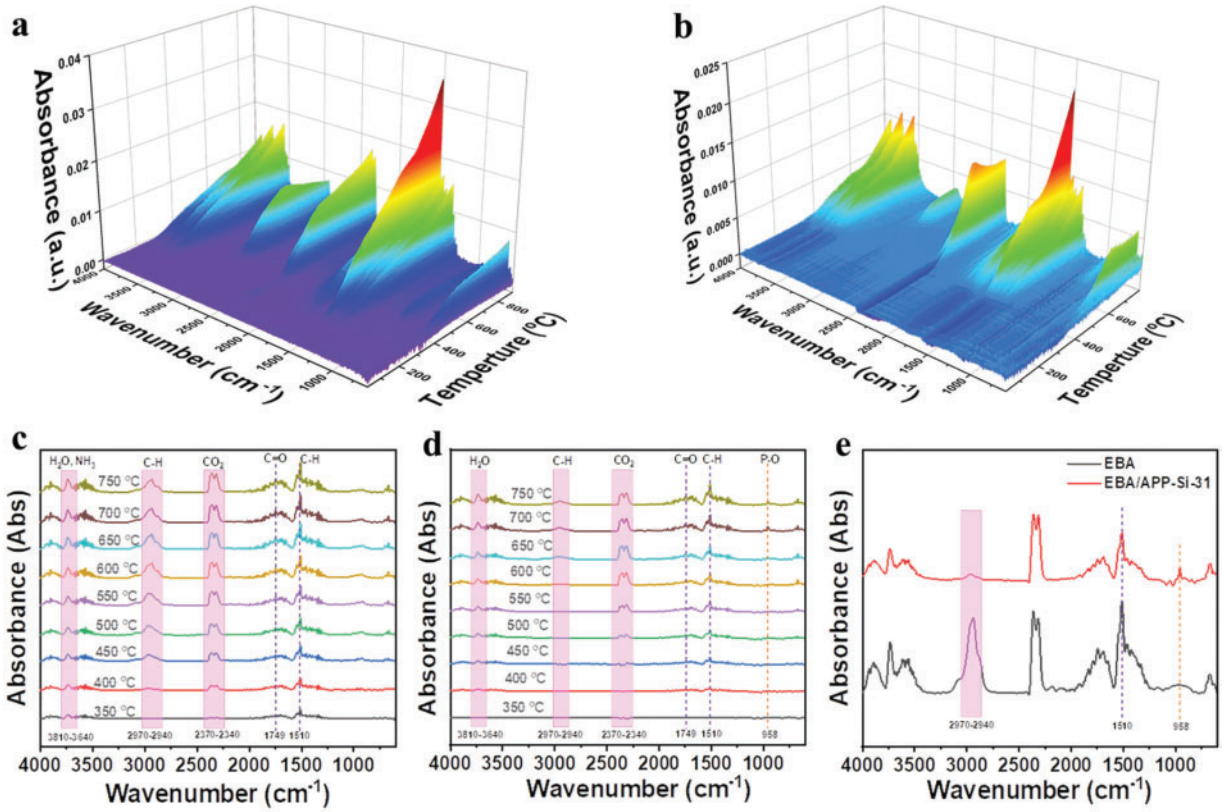

Figure 4: 3D TGA-FTIR images for (a) EBA and (b) EBA/APP-Si-31; FTIR spectra of gaseous products for (c) EBA and (d) EBA/APP-Si-31 at various temperatures, and (e) their FTIR spectra at the maximum degradation stage

The flame-retardant mechanism in the condensed phase was further investigated by analyzing the chars after cone calorimeter test, which were observed using a digital camera and SEM. In the case of EBA/APP, it exhibited a thin char layer with broken surfaces (Fig. 5a). In contrast, EBA/APP-Si-31 presented a dense char layer with interconnected surfaces (Fig. 5b). According to SEM images (Fig. 5c,d), the char layer of EBA/APP was composed of big holes, while the char of EBA/APP-Si-31 was a complete block without holes and cracks. These results indicated the char layer of EBA/APP-Si-31 had a better barrier effect in a fire.

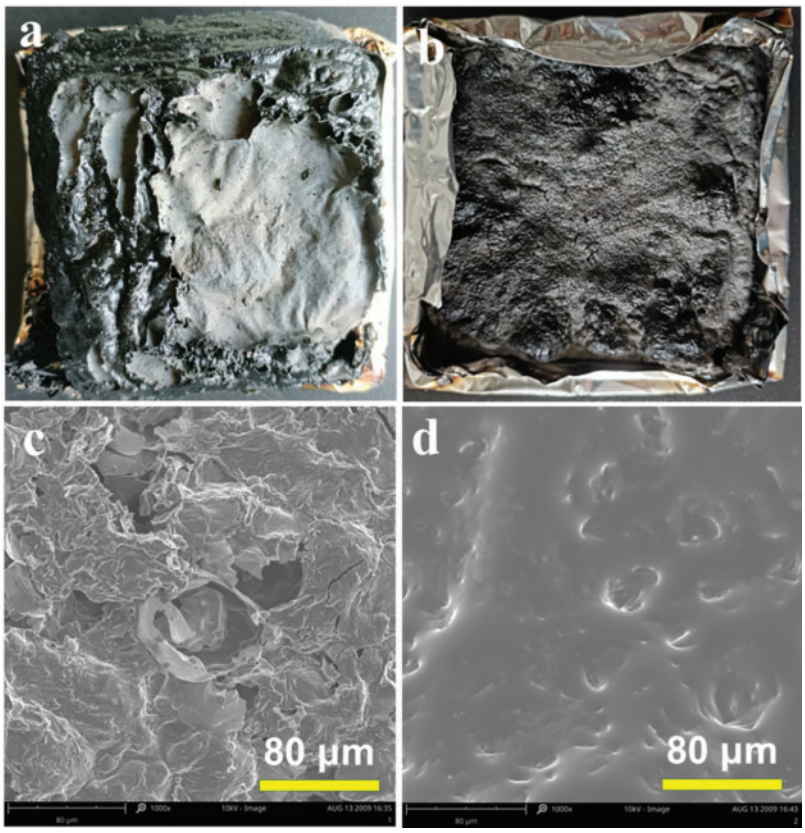

Figure 5: (a, b) Digital and (c, d) SEM images of char residues from EBA/APP and EBA/APP-Si-31

XPS was used to evaluate the elemental composition of residual chars. As shown in Fig. 6a, EBA/APP presented the characteristic peaks of P2s and P2p, which result from the thermal decomposition of APP. Besides P2s and P2p, the new peak of Si2p was detected in EBA/APP-Si-31, indicating that the Si-MCA participated in the construction of the char layer. In addition, the char residues were analyzed by FTIR (Fig. 6b). The typical bands from APP derivates were visible, including NH_4^+, P=O, P-O and P-C [28]. In the case of EBA/APP-Si-31, strong bands for C=N (1641 cm^{-1}) and Si-O (1022, 766, 478 cm^{-1}) were observed, which were attributed to the decomposition of Si-MCA [32].

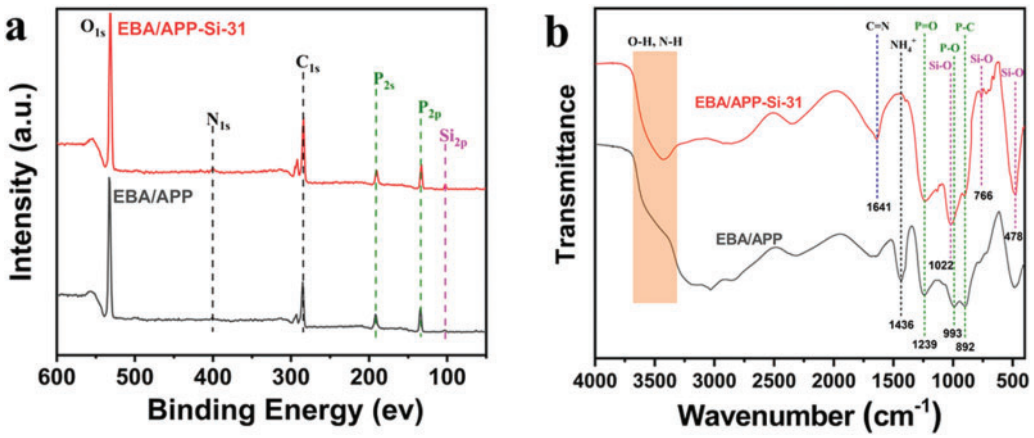

Figure 6: (a) XPS and (b) FTIR spectrums of char residues from EBA/APP and EBA/APP-Si-31

On the basis of the above analysis, Fig. 7a shows the chemical reaction between APP and Si-MCA. The decomposition of APP could release phosphoric acid [45], while Si-MCA could produce Si–OH. Their dehydration reactions (such as esterification) promoted the formation of cross-linking chains and further constructed intumescent char (C=N and P–O–Si). Meanwhile, lots of incombustible gases (NH_3, CO_2 and H_2O) were released. Moreover, a possible flame-retardant mechanism in EBA system was proposed. As illustrated in Fig. 7b, the combination of APP and Si-MCA as IFRs played important roles in gas phase and condensed phase during combustion. In gas zone, the thermal decomposition of APP produced PO•/HPO• radicals to quench H•/HO• radicals [28], and these non-flammable gases were helpful for diluting flammable gases and oxygen concentrations. In the condensed phase zone, the derivates from APP and Si-MCA constructed a continuous and compact char layer, which displayed excellent barrier effect to reduce the infiltration of heat and O_2 from outside as well as flammable gases from inside. Thus, the excellent flame retardancy in EBA composites with the LOI of 31.2%, the V0 rating in UL-94 and 76.4% reduction in PHRR was achieved.

3.3 Mechanical Properties of EBA/IFR Composites

As a useful polymer composite material for practical applications, it is highly desirable to achieve a balance between flame retardancy and mechanical performance [46–49]. The mechanical properties of EBA composites containing APP or APP/Si-MCA were evaluated by tensile testing. Fig. 8a shows the stress-strain curves of neat EBA and EBA composites, while the normalized values for Young's modulus, tensile strength and elongation at break are summarized in Fig. 8b. With the addition of 25 wt% APP, the Young's modulus of EBA/APP increased due to the reinforcing effect of rigid inorganic particles. However, the tensile strength and elongation at break significantly decreased in comparison with those of neat EBA. As for EBA/APP-Si-31 with the same total IFR content, it exhibited better mechanical properties than EBA/APP. The Young's modulus, tensile strength, and elongation at break increased by 6.2%, 7.6% and 12.3%, respectively. These results indicated the synergistic effect of APP/Si-MCA on improving the mechanical performance of EBA composites.

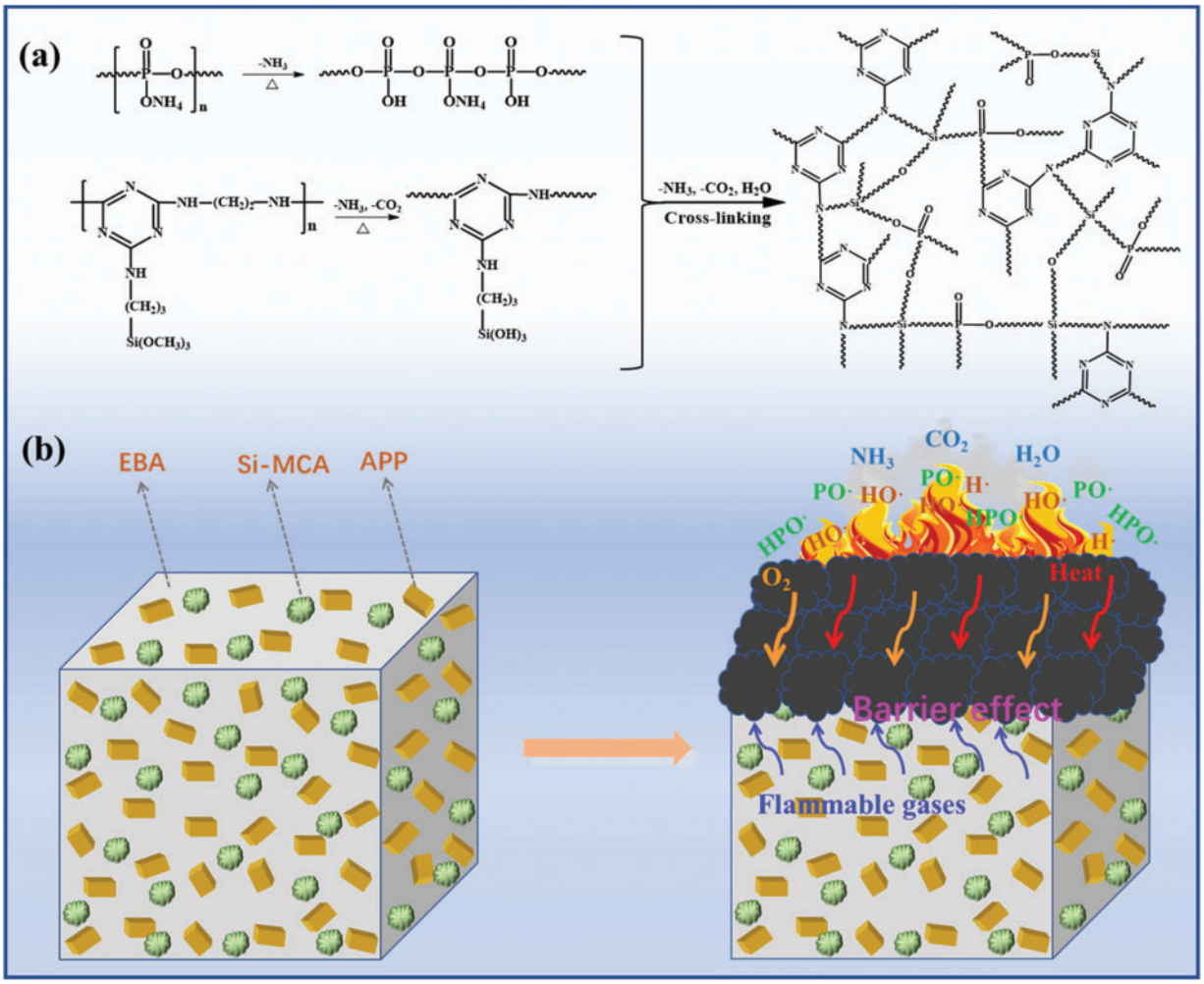

Figure 7: (a) The chemical reaction between APP and Si-MCA and (b) possible flame retardant mechanism of APP/Si-MCA in EBA composites

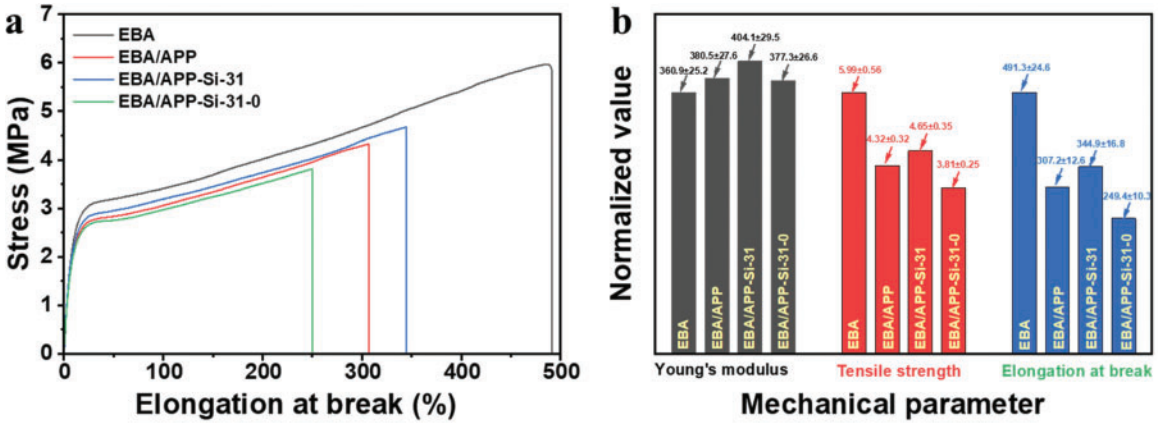

Figure 8: (a) Stress-strain curves and (b) normalized value of mechanical parameter for EBA composites

To investigate the effect of PE-*g*-MA on mechanical properties of the EBA system, EBA/APP/Si-MCA composites without PE-*g*-MA (denoted as EBA/APP-Si-31-0 in experimental section) were prepared under the same preparation conditions as EBA/APP-Si-31. It was found that all mechanical parameters of EBA/APP-Si-31-0 were lower than those of EBA/APP-Si-31 (Fig. 8a,b), including the Young's modulus (377.3 vs. 404.1 MPa), tensile strength (3.81 vs. 4.65 MPa), and elongation at break (249.4% vs. 344.9%). These results confirmed that PE-*g*-MA acted as an effective compatibilizer in EBA/IFR composites, which could improve the dispersion of fillers and the matrix-filler interaction [50,51]. As a result, EBA/APP-Si-31 presented relatively good mechanical properties with higher stiffness and toughness than EBA/APP-Si-31-0.

4 Conclusions

EBA/APP/Si-MCA composites were prepared by melt compounding with PE-*g*-MA as the compatibilizer, and the synergistic effect of APP/Si-MCA as IFRs on flame retardancy and mechanical properties of EBA composites was investigated. The optimal combination in EBA/APP-Si-31 exhibited the best flame retardancy with LOI of 31.2%, V0 rating in UL-94 test and 76.4% reduction in PHRR. The enhancement mechanism was attributed to the synergistic effect of APP/Si-MCA in the gas-phase and condensed-phase zones. Furthermore, EBA/APP-Si-31 also displayed better mechanical properties than other EBA composites. Specifically, EBA/APP-Si-31 had higher values on mechanical parameters than EBA/APP-Si-31-0, indicating the positive effect of PE-*g*-MA as a compatibilizer. This work indicates that APP/Si-MCA is an effective combination to achieve a good balance between flame retardancy and mechanical performance of EBA composites, which will promote the wider applications of EBA in cable and other fields.

Acknowledgement: The authors would like to thank Changchun Institute of Applied Chemistry, Chinese Academy of Sciences for cone calorimeter test.

Funding Statement: This work is supported by the National Natural Science Foundation of China (52473059), Taishan Scholar Constructive Engineering Foundation of Shandong Province (tsqn202103079) and Key Research and Development Plan of Shandong Province (2024TSGC0264).

Author Contributions: The authors confirm contribution to the paper as follows: fabricated and characterized the samples, wrote the original manuscript: Xuan Huo; data collection, analysis and interpretation of results: Bingchen Wu, Yuanmeng Lou, Junlin Zhu, Cui Li, Lili Ma; writing—review and editing, supervision: Ye-Tang Pan, Chuncheng Hao, Xin Wen. All authors reviewed the results and approved the final version of the manuscript.

Availability of Data and Materials: The datasets generated and/or analyzed during the current study are available from the corresponding authors on reasonable request.

Ethics Approval: Not applicable.

Conflicts of Interest: The authors declare no conflicts of interest to report regarding the present study.

References

1. Xu WZ, Cheng PF, Ding D, Zhang ZH, Bian ZW. Influence of BN doped 2-hydroxyethyl methacrylate phosphate coated expandable graphite on flame retardancy and thermal conductivity of styrene-butadiene rubber composites. Polym Adv Technol. 2023;34(10):3333–44. doi:10.1002/pat.6145.
2. Hedir A, Rondot S, Jbara O, Durmus A, Moudoud M, Lamrous O, et al. Assessment of UV-aging of crosslinked polyethylene cable insulation by electrical measurements, FTIR and DSC analyses. ECS J Solid State Sci Technol. 2025;14(1):013008. doi:10.1149/2162-8777/ada79e.
3. Li Y, Qi LJ, Liu YF, Qiao JJ, Wang MT, Liu XY, et al. Recent advances in halogen-free flame retardants for polyolefin cable sheath materials. Polymers. 2022;14(14):2876. doi:10.3390/polym14142876.

4. Gouda OE, Darwish MMF, Thabet A, Lehtonen M, Osman GFA. Enhancement of the underground cable current capacity by using nano-dielectrics. Energy Sci Eng. 2024;12(9):3647–62.
5. Zhang XB, Xu L, Sun Q, Zhang J, Sheng JW. Effect of crystalline phase formed by compound flame retardant on the flame retardancy and ceramization of polyethylene composites. Polym Adv Technol. 2024;35(6):e6485. doi:10.1002/pat.6485.
6. Fang Y, Hu D, Cao L, Tan WM, Tang C. Feature selection of XLPE cable condition diagnosis based on PSO-SVM. Arab J Sci Eng. 2023;48(5):5953–63. doi:10.1007/s13369-022-07175-9.
7. Meng XK, Yang H, Lu ZM, Liu YX. Study on catalytic pyrolysis and combustion characteristics of waste cable sheath with crosslinked polyethylene. Adv Compos Hybrid Mater. 2022;5(4):2948–63. doi:10.1007/s42114-022-00516-0.
8. Wang LC, Jia XF, Wang JP. Study on the flame retardancy of thermoplastic elastomers composites applied for cable sheath. Prog Rubber Plast Recycl Technol. 2025. doi:10.1177/14777606241313075.
9. Karthikeyan R, Rajkumar S, Ravi B. Effect of selective laser sintering polyamide-12 powder as a filler in glass fiber reinforced epoxy composites. J Polym Mater. 2024;41(3):131–41. doi:10.32604/jpm.2024.055989.
10. Hang AZ, Liu BB, Zhang CQ, Feng DL, Zhang EQ, Lv FZ, et al. Study on flame retardancy of melamine/g-C_3N_4 covalent organic framework nanosheets used in cable sheath material. AIP Adv. 2021;11(12):125109. doi:10.1063/5.0075195.
11. Wang P, Tian HY, Liu WX, Lu HB, Liu JJ, Dong S, et al. High-performance cable materials for maglev trains prepared by the multiple synergistic regulation effects of the functionalized ionic liquids on EVA-based composites. Adv Compos Hybrid Mater. 2024;7(4):107. doi:10.1007/s42114-024-00920-8.
12. Feng Y, Wang H, Zhang BX, Mo C, Dai YQ, Fan CY, et al. Effect of different surface modifiers on the flame retardancy of ethylene-vinyl acetate copolymer/polyethylene/magnesium hydroxide composite systems. Appl Polym Sci. 2024;141(41):e56061. doi:10.1002/app.56061.
13. Kerekes Z, Restás A, Lublóy É. The effects causing the burning of plastic coatings of fire-resistant cables and its consequences. J Therm Anal Calorim. 2020;139(2):775–87. doi:10.1007/s10973-019-08526-9.
14. Zhang Y, Chen XL, Fang ZP. Synergistic effects of expandable graphite and ammonium polyphosphate with a new carbon source derived from biomass in flame retardant ABS. J Appl Polym Sci. 2013;128(4):2424–32. doi:10.1002/app.38382.
15. Roda E, Galletti F, Truscello A, Gambarotti C. Flame behaviour of magnesium and aluminium hydroxide-filled polymer composites used in power and telecom cables. Plast Rubber Compos. 2022;51(4):185–95. doi:10.1080/14658011.2021.1962617.
16. Sabet M, Soleimani H, Hosseini S. Thermal stability and flame-retardant characteristic of irradiated LDPE and composites. Bull Mat Sci. 2020;43(1):38. doi:10.1007/s12034-019-2021-z.
17. Kaynak C, Ibibikcan E. Contribution of nanoclays to the flame retardancy of polyethylene-based cable insulation materials with aluminum hydroxide and zinc borate. J Fire Sci. 2014;32(2):121–44. doi:10.1177/0734904113500129.
18. Alosime EM, Basfar AA. A systematic investigation on the influence of intumescent flame retardants on the properties of ethylene vinyl acetate (EVA)/Liner low density polyethylene (LLDPE) blends. Molecules. 2023;28(3):1023. doi:10.3390/molecules28031023.
19. Makhlouf G, Hassan M, Nour M, Abdelmonem Y, Abdelkhalik A. A novel intumescent flame retardant: synthesis and its application for linear low-density polyethylene. Arab J Sci Eng. 2017;42(10):4339–49. doi:10.1007/s13369-017-2443-0.
20. Bellayer S, Dilger M, Duquesne S, Jimenez M. Flame-retardants for polypropylene: a review. Polym Degrad Stab. 2024;230(8):111008. doi:10.1016/j.polymdegradstab.2024.111008.
21. Paszkiewicz S, Irska I, Taraghi I, Piesowicz E, Sieminski J, Zawisza K, et al. Halloysite nanotubes and silane-treated alumina trihydrate hybrid flame retardant system for high-performance cable insulation. Polymers. 2021;13(13):2134. doi:10.3390/polym13132134.
22. Chen H, Wen X, Guan YY, Min JK, Wen YL, Yang HF, et al. Effect of particle size on the flame retardancy of poly(butylene succinate)/$Mg(OH)_2$ composites. Fire Mater. 2016;40(8):1090–6. doi:10.1002/fam.2355.
23. Wang Z, Qu B, Fan W, Huang P. Combustion characteristics of halogen-free flame-retarded polyethylene containing magnesium hydroxide and some synergists. J Appl Polym Sci. 2001;81(1):206–14. doi:10.1002/app.1430.

24. Ye L, Miao Y, Yan H, Li Z, Zhou Y, Liu J, et al. The synergistic effects of boroxo siloxanes with magnesium hydroxide in halogen-free flame retardant EVA/MH blends. Polym Degrad Stab. 2013;98(4):868–74. doi:10.1016/j.polymdegradstab.2013.01.001.
25. Tian S, He H, Wang D, Yu P, Jia Y, Luo Y. Study of using aluminum hypophosphite as a flame retardant for low-density polyethylene. Fire Mater. 2017;41(8):983–92. doi:10.1002/fam.2443.
26. Liang JZ, Feng JQ, Tsui CP, Tang CY, Huang WF. Mechanical properties and morphology for polypropylene composites filled with microencapsulated red phosphorus. Polym Adv Technol. 2014;25(3):347–52. doi:10.1002/pat.3248.
27. Wang DK, He H, Yu P. Flame-retardant and thermal degradation mechanism of low-density polyethylene modified with aluminum hypophosphite and microencapsulated red phosphorus. J Appl Polym Sci. 2016;133(13):43225. doi:10.1002/app.43225.
28. Yang H, Guan Y, Ye L, Wang S, Li S, Wen X, et al. Synergistic effect of nanoscale carbon black and ammonium polyphosphate on improving thermal stability and flame retardancy of polypropylene: a reactive network for strengthening carbon layer. Compos Part B-Eng. 2019;174(5):107038. doi:10.1016/j.compositesb.2019.107038.
29. Khanal S, Zhang W, Ahmed S, Ali M, Xu S. Effects of intumescent flame retardant system consisting of tris (2-hydroxyethyl) isocyanurate and ammonium polyphosphate on the flame retardant properties of high-density polyethylene composites. Compos Part A-Appl S. 2018;112(3):444–51. doi:10.1016/j.compositesa.2018.06.030.
30. Zhang N, Zhang J, Yan H, Guo X, Sun Q, Guo R. A novel organic-inorganic hybrid K-HBPE@APP performing excellent flame retardancy and smoke suppression for polypropylene. J Hazard Mater. 2019;373:856–65. doi:10.1016/j.jhazmat.2019.04.016.
31. Ren Y, Yuan D, Li W, Cai X. Flame retardant efficiency of KH-550 modified urea-formaldehyde resin cooperating with ammonium polyphosphate on polypropylene. Polym Degrad Stab. 2018;151(6):160–71. doi:10.1016/j.polymdegradstab.2018.03.014.
32. Guan Y, Wen X, Yang H, Zhang L, Li M, Shao J, et al. One-pot synthesis of crosslinked silicone-containing macromolecular charring agent and its synergistic flame retardant poly(l-lactic acid) with ammonium polyphosphate. Polym Adv Technol. 2017;28(11):1409–17. doi:10.1002/pat.4017.
33. Xiong ZQ, Zhang Y, Du XY, Song PA, Fang ZP. Green and scalable fabrication of core-shell biobased flame retardants for reducing flammability of polylactic acid. ACS Sustain Chem Eng. 2019;7(9):8954–63. doi:10.1021/acssuschemeng.9b01016.
34. Li Z, Huang GB, Li H, Zhang L, Liu ZQ, de la Vega J, et al. Fire-safe and multifunctional epoxy/layered double hydroxide composites via an interfacial catalysis. Appl Clay Sci. 2024;260:107545. doi:10.1016/j.clay.2024.107545.
35. Yu YM, Zhang Y, Xi LD, Zhao ZN, Huo SQ, Huang GB, et al. Interface nanoengineering of a core-shell structured biobased fire retardant for fire-retarding polylactide with enhanced toughness and UV protection. J Cleaner Prod. 2022;336(12):130372. doi:10.1016/j.jclepro.2022.130372.
36. Ma CC, Zhang Y, Zhao ZN, Wang JW, Chen YJ, Qian LJ, et al. Green synthesis of bio-based flame retardant/natural rubber inorganic-organic hybrid and its flame retarding and toughening effect for polylactic acid. Int J Biol Macromol. 2024;256(9):128378. doi:10.1016/j.ijbiomac.2023.128378.
37. Yang JX, Sun Y, Song WM, Liu Y. A novel phosphorus/boron-containing flame retardant for improving the flame retardancy of ramie fiber reinforced epoxy composites. Constr Build Mater. 2024;451(15):138814. doi:10.1016/j.conbuildmat.2024.138814.
38. Makhlouf G, Abdelkhalik A, Hassan MA. Combustion toxicity of polypropylene containing melamine salt of pentaerythritol phosphate with high efficiency and stable flame retardancy performance. Process Saf Environ Protect. 2020;138(6):300–11. doi:10.1016/j.psep.2020.04.012.
39. Zhang Y, Xiong ZQ, Ge HD, Ni LK, Zhang T, Huo SQ, et al. Core-shell bioderived flame retardants based on chitosan/alginate coated ammonia polyphosphate for enhancing flame retardancy of polylactic acid. ACS Sustain Chem Eng. 2020;8(16):6402–12. doi:10.1021/acssuschemeng.0c00634.
40. Beyer G. Flame retardant properties of EVA-nanocomposites and improvements by combination of nanofillers with aluminium trihydrate. Fire Mater. 2001;25(5):193–7. doi:10.1002/fam.776.

41. Wang D, Wen X, Chen X, Li Y, Mijowska E, Tang T. A novel stiffener skeleton strategy in catalytic carbonization system with enhanced carbon layer structure and improved fire retardancy. Compos Sci Technol. 2018;164(48):82–91. doi:10.1016/j.compscitech.2018.05.040.
42. Ma L, Liu H, Wen X, Szymańska K, Mijowska E, Hao C, et al. Polyhydric SiO_2 coating assistant to graft organophosphorus onto glass fabric for simultaneously improving flame retardancy and mechanical properties of epoxy resin composites. Compos Part B-Eng. 2022;243(15):110176. doi:10.1016/j.compositesb.2022.110176.
43. Li C, Long Y, Lou Y, Huo X, Ma L, Tang Y, et al. Three-in-one novel flame retardant through grafting organophosphorus onto Fe-MOF functionalized $Mg(OH)_2$ for improving fire safety and mechanical properties of PBS composites. Sustainable Mater Technol. 2024;40:e00906. doi:10.1016/j.susmat.2024.e00906.
44. Li C, Ba Z, Wu B, Shi X, Liu H, Ma L, et al. Bio-inspired construction of hydrophobic $Mg(OH)_2$/Co-MOF/DOPO hybrids for simultaneously improving flame retardancy and mechanical properties of poly(L-lactic acid) composites. Chem Eng J. 2025;504(42):158853. doi:10.1016/j.cej.2024.158853.
45. Hang Y, Liu LH, Yao MH, Feng JB, Xue YJ, Annamalai PK, et al. Functionalizing lignin by *in situ* solid-phase grafting ammonium polyphosphate for enhancing thermal, flame-retardant, mechanical, and UV-resistant properties of polylactic acid. Chem Eng J. 2024;495:153429. doi:10.1016/j.cej.2024.153429.
46. Yao MH, Liu LH, Ma CC, Zhang H, Zhang Y, Song RY, et al. A lysine-derived flame retardant for improved flame retardancy, crystallinity, and aqueous-phase degradation of polylactide. Chem Eng J. 2023;462(1):142189. doi:10.1016/j.cej.2023.142189.
47. Jing J, Zhang Y, Fang ZP, Wang DY. Core-shell flame retardant/graphene oxide hybrid: a self-assembly strategy towards reducing fire hazard and improving toughness of polylactic acid. Compos Sci Technol. 2018;165:161–7. doi:10.1016/j.compscitech.2018.06.024.
48. Liu LH, Yao MH, Zhang H, Zhang Y, Feng JB, Fang ZP, et al. Aqueous self-assembly of bio-based flame retardants for fire-retardant, smoke-suppressive, and toughened polylactic acid. ACS Sustain Chem Eng. 2022;10(49):16313–23. doi:10.1021/acssuschemeng.2c05298.
49. Zhang Y, Jing J, Liu T, Xi LD, Sai T, Ran SY, et al. A molecularly engineered bioderived polyphosphate for enhanced flame retardant, UV-blocking and mechanical properties of poly(lactic acid). Chem Eng J. 2021;411(7):128493. doi:10.1016/j.cej.2021.128493.
50. Wang YM, Meng FJ, Zhu JL, Ba ZT, Jiang DY, Wen X, et al. Synergistic effect of carbon nanotube on improving thermal stability, flame retardancy, and electrical conductivity of poly(butylene succinate)/piperazine pyrophosphate composites. Colloid Polym Sci. 2023;301(12):1529–37. doi:10.21203/rs.3.rs-3214645/v1.
51. Wen X, Liu Z, Li Z, Zhang J, Wang D-Y, Szymańska K, et al. Constructing multifunctional nanofiller with reactive interface in PLA/CB-g-DOPO composites for simultaneously improving flame retardancy, electrical conductivity and mechanical properties. Compos Sci Technol. 2020;188(3):107988. doi:10.1016/j.compscitech.2019.107988.